Differences in fracture healing between female and male C57BL/6J mice

Melanie Haffner-Luntzer (melanie.haffner-luntzer@uni-ulm.de)
Universitatsklinikum Ulm https://orcid.org/0000-0002-3333-2613
Verena Fischer
Universitätsklinik Ulm
Anita Ignatius
Universitätsklinikum Ulm

Research

Keywords: fracture healing, mouse model, estrogen, sex-related differences

Posted Date: November 13th, 2020

DOI: https://doi.org/10.21203/rs.3.rs-106980/v1

Abstract

Background: Mice are increasingly used in fracture healing research because of the opportunity to use transgenic animals. While both, male and female mice are employed, there is no consensus in the literature whether fracture healing differs between both sexes. Therefore, the aim of the present study was to analyse diaphyseal fracture healing in female and male C57BL/6J mice, a commonly used mouse strain in bone research.

Methods: For that purpose, 12-week-old female (17–20 g) and male mice (22–26 g) received a standardised femur midshaft osteotomy stabilised by an external fixator. Mice were euthanized 10 and 21 days after fracture and bone healing was analysed by biomechanical testing, µCT, histology, immunohistochemistry and qPCR.

Results: Ten days after fracture, male mice displayed significantly more cartilage but less fibrous tissue in the fracture callus compared to female mice, whereas the amount of bone did not differ. At day 21, male mice showed a significantly larger fracture callus compared to female mice. The relative amount of bone in the fracture callus did not significantly differ between both sexes, whereas its tissue mineral density was significantly higher in male mice on day 21, indicating more mature bone and slightly more rapid fracture healing. These results were confirmed by a significantly greater absolute bending stiffness of the fractured femurs of male mice on day 21. On the molecular level, male mice displayed increased active β-catenin expression in the fracture callus, whereas oestrogen receptor α (ERα) expression was lower.

Conclusions: These results suggest that male mice display more rapid fracture healing with more prominent cartilaginous callus formation. This might be due to the higher weight of male mice, resulting in increased mechanical loading of the fracture. Furthermore, male mice displayed significantly greater activation of osteoanabolic Wnt/β-catenin signalling, which might also contribute to more rapid bone regeneration.

Introduction

Fracture healing is a highly regulated and complex process involving many cell types and signalling pathways, but remains insufficiently understood. To analyse the bone healing process in molecular detail, animal models in which it is possible to induce or delete specific factors involved during the healing cascade are needed. For this reason, mice have become increasingly popular for fracture healing research in recent years, because there are manifold transgenic strains available. Thereby, it has to be taken into consideration that bone regeneration differs between young and old mice [1–5] and between different strains [1, 6]. Regarding sex differences, the literature is strongly debated. Some authors report more rapid bone regeneration in male rats and mice compared to females [7, 8]. However, there are also studies showing no sex-specific differences in murine fracture healing [9, 10]. In many studies, data generated from female and male mice are pooled together, simply stipulating that there would be no sex-specific difference in the healing process. However, it is known that sex hormones like oestrogen have

considerable effects on bone healing [11–13]. There are also clinical indications that male patients display more rapid fracture healing and that women may have an increased risk for atrophic non-unions rather than hypertrophic non-unions as observed in males [14, 15]. By contrast, there are also clinical studies reporting no influence of sex on fracture healing in specific fracture types [16–18].

The aim of this study was to analyse the similarities and differences in diaphyseal fracture healing between 12-week-old female and male C57BL/6J mice. We chose this mouse model, because this mouse strain of this age is frequently used in bone healing research.

Material And Methods

Animals and experimental design

All experiments were performed according to German Guidelines for Animal Research on the Protection of Animals as well as the ARRIVE guidelines and were approved by the local ethical committee (No. 1026, 1096, 1219, Regierungspräsidium Tübingen, Germany). Ten-week-old male and female C57BL/6J mice were purchased from Charles River laboratories. Following an acclimatisation time period of 2 weeks, 12-week-old mice were subjected to a unilateral femoral midshaft osteotomy stabilised by an external fixator. Mice were euthanized at day 10 and 21 after fracture and bones were analysed by biomechanical testing, µCT analysis, histology and gene expression analysis.

Mice were maintained under standard laboratory conditions with up to five animals per cage on a 14 h light and 10 h dark rhythm with water and food available *ad libitum*. All mice received the same standard diet (R/M-H, V1535-300, Ssniff Spezialitäten GmbH). The female mice weighed 17–20 g on the day of the surgery, while the male mice weighed 22–26 g.

Surgical procedure

Surgery was performed under general anaesthesia with 2% isoflurane (Forene, Abbott). The fracture healing model was previously described in detail [19]. Briefly, a standardised osteotomy gap was created at the midshaft of the right femur using a 0.4 mm wire saw (RISystem) and stabilised by an external fixator (axial stiffness 3.0 N/mm, RISystem). The mice received as analgesia 25 mg/L tramalhydrochloride (Tramal, Gruenenthal GmbH) in the drinking water 1 day preoperatively until 3 days postoperatively.

Biomechanical testing

Fractured and intact femurs were harvested 21 days after surgery, muscles were removed and specimens were stored in saline solution until biomechanical testing. Testing was performed on the same day of euthanasia as described previously [20]. Briefly, bones were embedded into aluminium cylinders at the proximal end and loaded in a materials testing machine (Zwick, Germany). A maximum load of 4 N for intact and 2 N for fractured femurs was applied and the load-deflection curve was recorded. Bending stiffness was calculated from the slope of this curve. Relative bending stiffness was calculated using the values from the fractured and intact femur from the same animal. Some of the biomechanical

parameters were already published in another context, because the mice used for this study served as control groups in previous studies [21, 22].

µCT analysis

Following biomechanical testing, the proximal end of the femurs was cut and specimens were fixed in 4% buffered formalin. Fixed samples were scanned using an isotrophic resolution of 8 µm and standard µCT settings of 200 mA and 50 kV in a µCT scanning device (Skyscan 1172). Fracture callus parameters were analysed from the entire tissue between the two fractured cortices with a threshold of 642 mg hydroxyapatite/cm^3.

Histological analysis

Following 48 h of fixation, bones from day 10 post fracture were decalcified and embedded in paraffin as described previously [20]. Bones from day 21 post fracture were embedded undecalcified in methacrylate. Sections of 7 µm were cut and stained with Safranin O (decalcified) or Giemsa (undecalcified) or for tartrate-resistant alkaline phosphatase (TRAP). The amounts of bone, cartilage and fibrous tissue in the fracture callus were determined by Safranin O or Giemsa staining using image analysis software (Leica DMI6000 B; Software MMAF Version 1.4.0). Regions of interest were the fracture callus between the two inner pin holes on day 10 and between the two fractured cortices on day 21. The number and surface of osteoblasts (NOb/BPm, ObS/BS, respectively) were determined in Safranin O- or Giemsa-stained sections. The number and surface of osteoclasts (NOc/BPm, OcS/BS, respectively) were determined after TRAP staining. Bone cells and surface were evaluated using Osteomeasure software (Osteometrics) according to ASBMR standards. Regions of interest are indicated in Figs. 1 and 4, respectively.

Immunohistochemical staining

Paraffin-embedded 7 µm longitudinal sections were prepared for immunohistochemical staining, using the following antibodies and dilutions: rabbit anti-mouse non-phospho (active) beta-catenin (#8814, CellSignaling 1:50), rabbit anti-mouse ERalpha (#sc-542, Santa Cruz 1:75), rabbit anti-mouse ERbeta (#sc-8974, Santa Cruz 1:40) and goat-anti rabbit IgG-biotin (sc-3840, Santa Cruz 1:100), and horseradish peroxidase (HRP)-conjugated streptavidin (Zytomed Systems). 3-Amino-9-ethylcarbazol (Zytomed Systems) was used as the chromogen. Sections were counterstained using haematoxylin (Waldeck). Species-specific non-targeting immunoglobulins were used as isotype controls.

Gene expression analysis

RNA was isolated from 15 µm paraffin sections (three sections per mouse) using the RNEasy FFPE kit (Qiagen) according to the manufacturer's instructions. The amount and purity of RNA was measured photometrically with a Tecan NanoPlate. Quantitative PCR was performed using the SensiFAST SYBR Hi-ROX One-Step Kit (Bioline) according to the manufacturer's instructions. *B2M* was used as the housekeeping gene (F: 5'-ccc gcc tca cat tga aat cc-3', R: 5'-tgc tta act ctg cag gcg tat-3'). Relative gene expression of *Esr1* (F: 5'-tcc ggc aca tga gta aca aa-3', R: 5'-cca gga gca ggt cat aga gg-3') and *Esr2* (F: 5'-gag tag ccg gaa gct gac ac-3', R: 5'-tct tca aaa tca ccc aga cc-3') was calculated using the delta-delta CT method.

Statistics

Data were tested for normal distribution using the Shapiro-Wilk normality test. Most datasets were normally distributed. Therefore, results are presented as bars with mean ± standard deviation. Statistical analysis was performed by Student's t-test (GraphPad Prism 9). The level of significance was set at $p < 0.05$. Group size was 6–8, and was calculated based on the findings of a previous fracture healing study with the main outcome parameters of flexural rigidity and BV/TV in the fracture callus [23].

Results

All mice displayed normal limb loading within the first 3 days after fracture. No animals were lost due to anaesthesia or surgical issues. At day 10 after fracture, the callus size did not significantly differ between female and male mice (Fig. 1A). Additionally, the bone content of the fracture callus did not differ between both sexes (Fig. 1B). However, the fibrous tissue fraction was significantly lower, whereas the cartilage fraction was significantly higher in male mice (Fig. 1C–E). There were no significant differences in osteoblast or osteoclast numbers or surface between female and male mice (Fig. 1F–J). Immunohistochemical staining revealed that active β-catenin, a marker for activated Wnt-signalling, was highly expressed in osteoblasts and proliferating chondrocytes in the fracture callus, whereas hypertrophic chondrocytes displayed no or only less expression (Fig. 2A). Although this expression pattern was found in both sexes, the staining intensity was much stronger in male animals. ERα was expressed in osteoblasts and chondrocytes in the fracture callus of female and male mice, however, its expression particularly in hypertrophic chondrocytes was lower in male mice (Fig. 2B). ERβ was expressed in osteoblasts and chondrocytes in the fracture callus with no obvious differences between both sexes (Fig. 2C). Gene expression analysis of fractured femurs confirmed significantly lower ERα expression in male mice (Fig. 2D). No differences were detected in ERβ gene expression (Fig. 2E).

On day 21, µCT analysis revealed a significantly larger fracture callus in male compared to female mice (Fig. 3A, B). By contrast, the bone volume to tissue volume ratio did not differ between both sexes, whereas the tissue mineral density of the newly formed bone was significantly higher in male mice (Fig. 3D, E). Biomechanical testing analysis revealed a greater bending stiffness of fractured and intact femurs in male mice (Fig. 3F, G). Histomorphometrical analysis confirmed that the callus was significantly larger in male mice (Fig. 4A), whereas the relative bone area, fibrous tissue area and cartilage area did not differ (Fig. 4B–E). At the bone trabeculae, the osteoclast number and surface were significantly greater in male mice compared with females (Fig. 4I–K), whereas osteoblast number and surface did not differ between both sexes (Fig. 4F, G).

Discussion

The aim of the present study was to shed light on the question of whether the fracture healing process differs between female and male C57BL/6J mice. Our data suggest a slightly more rapid fracture healing with a more prominent cartilaginous callus formation in male compared to female mice.

On day 21, the time point of bony bridging of the fracture gap, the absolute bending stiffness of the fracture callus was significantly greater in male mice. However, because the absolute bending stiffness of the intact femur was also greater in male mice, relative values did not differ between both sexes. Male mice display stronger bones than female mice because of greater cortical width [24]. The greater absolute bending stiffness of the fractured femurs of male mice might be caused by the significantly greater fracture callus size, which might result from the larger dimensions of the femur and greater mechanical loading of the fractured femur. Callus development highly depends on the interfragmentary strains in the fracture area [25–27]. The higher body weight in male mice might have resulted in a stronger deformation of the used semi-rigid external fixator during limb loading, resulting in greater interfragmentary strains. Larger fracture calli in male mice compared to female mice were also found in a study using a tibia fracture model with intramedullary stabilisation [8], whereas others did not detect differences between male and female mice regarding callus size in a similar model [9].

Furthermore, we found that the relative bone volume in the fracture callus did not differ between female and male mice. However, male mice displayed higher tissue mineral density, indicating a more mature bone in the fracture callus and further supporting a slightly more rapid fracture healing process, although osteoblast number and activity did not differ. By contrast, osteoclast number and activity were significantly increased in the fracture callus of male mice. This is surprising, because one would suggest that more osteoclasts would lead to more rapid callus remodelling, whereas, male mice displayed larger fracture calli at this time point. It would be of interest to include more time points during the late phase of fracture healing to investigate the kinetics of osteoclast differentiation and callus remodelling. Deng et al. found more osteoclasts in the fracture callus of female mice 6 weeks after fracture [8]. Therefore, it is likely that osteoclast formation and callus remodelling differ between both sexes.

During the intermediate phase of endochondral fracture healing at day 10 after surgery, male mice displayed a similar callus size compared to female mice, however, the cartilage content was significantly greater in male mice, whereas the amount of fibrous tissue was significantly lower. This indicates more rapid cartilaginous callus development in male mice. One reason might be the already mentioned differences in the biomechanical environment at the fracture site. Furthermore, on the molecular level, male mice displayed greater activation of the osteoanabolic Wnt/β-catenin signalling pathway in the fracture callus. Because inhibition of this pathway specifically in chondrocytes led to delayed cartilaginous callus formation during fracture healing [28], altered Wnt/β-catenin signalling might play a role here. Another difference between male and female mice was found regarding ERα expression in the fracture callus. Male mice displayed significantly less ERα expression than female mice, particularly in hypertrophic chondrocytes. This might also account for the differences found in cartilaginous callus formation, because oestrogen-dependent ERα signalling was shown to be important for the regulation of chondrocyte differentiation during endochondral ossification [29]. Studies investigating mechanistic differences in fracture healing between male and female mice are generally lacking. One study suggested that male rats exhibit more mesenchymal stem cells in the bone marrow compared to female rats and that this might account for more rapid fracture healing in male rodents [30].

Clinical studies analysing differences in fracture healing between male and female fracture patients are rather rare and results are difficult to interpret, because other influencing factors, including fracture type, degree of tissue trauma, body weight and clinical manifestation of osteoporosis, frequently differ between men and women. It was shown for some types of fractures that male patients displayed more rapid fracture healing and women had an increased risk for atrophic non-unions rather than hypertrophic non-unions in males [14, 15]. One clinical study reported significantly increased blood levels of the Wnt/β-catenin-signalling inhibitor Sclerostin in male geriatric hip fracture patients compared to female age-matched patients, whereas the concentrations of another Wnt/β-catenin-signalling inhibitor, Dickkopf-1 were reduced [31]. When comparing male fracture patients to postmenopausal female fracture patients, men displayed significantly lower systemic levels of the inflammatory cytokine and Wnt/β-catenin-signalling inhibitor Midkine during long bone fracture healing [12]. Concluding, systemic concentrations of Wnt/β-catenin-signalling inhibitors appear to be different between male and female fracture patients, however, the underlying mechanisms have to date been minimally investigated.

In summary, the present study demonstrated specific differences in the endochondral fracture healing process between male and female mice, with male mice displaying a more rapid fracture healing process. Limitations of this study are that we did not analyse further time points during fracture healing and that we focused on only specific pathways which we hypothesized might be altered between the two sexes, namely Wnt/β-catenin and ER signalling. Further unbiased analyses of other pathways involved in the fracture healing process would be desirable. Nevertheless, this study suggests that the sex of the mice is relevant in fracture healing research and that data from male and female mice should not be pooled together.

Declarations

Ethics approval and consent to participate

All experiments were performed according to the German Guidelines for Animal Research on the Protection of Animals as well as the ARRIVE guidelines and were approved by the local ethical committee (No. 1026, 1096, 1219, Regierungspräsidium Tübingen, Germany)

Consent for publications

Not applicable

Availability of data and materials

The datasets supporting the conclusions of this article are included within the article.

Competing interests

The authors have declared that no conflict of interest exists.

Funding

This work was performed within the framework of the CRC1149, funded by the German Research Foundation (project number 251293561: INST 40/599-1 and INST 40/491-2). The funding body does not have any role in the design of the study, collection, analysis or interpretation of data or in writing the manuscript.

Author contributions

MHL, VF: conducting experiments. MHL, AI: substantial contributions to research design. MHL, VF, AI: interpretation of data. MHL: drafting the paper. All authors: revising the paper critically and approval of the submitted version.

Acknowledgement

We thank Iris Baum, Kristina Diepold and Yasemine Aydoglu for excellent technical assistance. This work was performed within the framework of the CRC1149, funded by the German Research Foundation (project number 251293561: INST 40/599-1 and INST 40/491-2).

References

[1] M. Haffner-Luntzer, A. Kovtun, A.E. Rapp, A. Ignatius, Mouse Models in Bone Fracture Healing Research, Current Molecular Biology Reports 2(2) (2016) 101-111.

[2] C. Lu, E. Hansen, A. Sapozhnikova, D. Hu, T. Miclau, R.S. Marcucio, Effect of age on vascularization during fracture repair, Journal of orthopaedic research : official publication of the Orthopaedic Research Society 26(10) (2008) 1384-9.

[3] C. Lu, T. Miclau, D. Hu, E. Hansen, K. Tsui, C. Puttlitz, R.S. Marcucio, Cellular basis for age-related changes in fracture repair, Journal of orthopaedic research : official publication of the Orthopaedic Research Society 23(6) (2005) 1300-7.

[4] D. Clark, M. Nakamura, T. Miclau, R. Marcucio, Effects of Aging on Fracture Healing, Curr Osteoporos Rep 15(6) (2017) 601-608.

[5] A.M. Josephson, V. Bradaschia-Correa, S. Lee, K. Leclerc, K.S. Patel, E. Muinos Lopez, H.P. Litwa, S.S. Neibart, M. Kadiyala, M.Z. Wong, M.M. Mizrahi, N.L. Yim, A.J. Ramme, K.A. Egol, P. Leucht, Age-related inflammation triggers skeletal stem/progenitor cell dysfunction, Proc Natl Acad Sci U S A 116(14) (2019) 6995-7004.

[6] M.B. Manigrasso, J.P. O'Connor, Comparison of fracture healing among different inbred mouse strains, Calcif Tissue Int 82(6) (2008) 465-74.

[7] M. Mehta, H. Schell, C. Schwarz, A. Peters, K. Schmidt-Bleek, A. Ellinghaus, H.J. Bail, G.N. Duda, J. Lienau, A 5-mm femoral defect in female but not in male rats leads to a reproducible atrophic non-union, Arch Orthop Trauma Surg 131(1) (2011) 121-9.

[8] Z. Deng, X. Gao, X. Sun, Y. Cui, S. Amra, J. Huard, Gender differences in tibial fractures healing in normal and muscular dystrophic mice, Am J Transl Res 12(6) (2020) 2640-2651.

[9] C.D. Collier, B.S. Hausman, S.H. Zulqadar, E.S. Din, J.M. Anderson, O. Akkus, E.M. Greenfield, Characterization of a reproducible model of fracture healing in mice using an open femoral osteotomy, Bone Rep 12 (2020) 100250.

[10] Z.M. Working, E.R. Morris, J.C. Chang, R.F. Coghlan, B. Johnstone, T. Miclau, 3rd, W.A. Horton, C.S. Bahney, A quantitative serum biomarker of circulating collagen X effectively correlates with endochondral fracture healing, Journal of orthopaedic research : official publication of the Orthopaedic Research Society (2020).

[11] M. Haffner-Luntzer, V. Fischer, K. Prystaz, A. Liedert, A. Ignatius, The inflammatory phase of fracture healing is influenced by oestrogen status in mice, European Journal of Medical Research 22 (2017).

[12] V. Fischer, M. Kalbitz, F. Muller-Graf, F. Gebhard, A. Ignatius, A. Liedert, M. Haffner-Luntzer, Influence of Menopause on Inflammatory Cytokines during Murine and Human Bone Fracture Healing, Int J Mol Sci 19(7) (2018).

[13] F.T. Beil, F. Barvencik, M. Gebauer, S. Seitz, J.M. Rueger, A. Ignatius, P. Pogoda, T. Schinke, M. Amling, Effects of estrogen on fracture healing in mice, J Trauma 69(5) (2010) 1259-65.

[14] M. Rupp, S. Kern, T. El Khassawna, A. Ismat, D. Malhan, V. Alt, C. Heiss, M.J. Raschke, Do Systemic Factors Influence the Fate of Nonunions to Become Atrophic? A Retrospective Analysis of 162 Cases, Biomed Res Int 2019 (2019) 6407098.

[15] X.P. Li, X.Y. Li, M.H. Yang, S.W. Zhu, X.B. Wu, P. Zhang, Changes of bone turnover markers after elderly hip fracture surgery, J Bone Miner Metab (2020).

[16] G. Lofrese, A. Musio, F. De Iure, F. Cultrera, A. Martucci, C. Iaccarino, W. Essayed, R. Ghadirpour, F. Servadei, M.A. Cavallo, P. De Bonis, Type II odontoid fracture in elderly patients treated conservatively: is fracture healing the goal?, Eur Spine J 28(5) (2019) 1064-1071.

[17] R. Morochovic, K. Takacova, L. Tomcovcik, P. Cibur, R. Burda, Factors influencing femoral neck fracture healing after internal fixation with dynamic locking plate, Arch Orthop Trauma Surg 139(5) (2019) 629-638.

[18] J.P. Johnson, J. Kleiner, A.D. Goodman, J.A. Gil, A.H. Daniels, R.A. Hayda, Treatment of femoral neck fractures in patients 45-64 years of age, Injury 50(3) (2019) 708-712.

[19] V. Röntgen, R. Blakytny, R. Matthys, M. Landauer, T. Wehner, M. Göckelmann, P. Jermendy, M. Amling, T. Schinke, L. Claes, A. Ignatius, Fracture healing in mice under controlled rigid and flexible conditions using an adjustable external fixator, Journal of orthopaedic research : official publication of the Orthopaedic Research Society 28(11) (2010) 1456-62.

[20] M. Haffner-Luntzer, A. Heilmann, A.E. Rapp, R. Roessler, T. Schinke, M. Amling, A. Ignatius, A. Liedert, Antagonizing midkine accelerates fracture healing in mice by enhanced bone formation in the fracture callus, Br J Pharmacol 173(14) (2016) 2237-49.

[21] A. Heilmann, T. Schinke, R. Bindl, T. Wehner, A. Rapp, M. Haffner-Luntzer, A. Liedert, M. Amling, A. Ignatius, Systemic treatment with the sphingosine-1-phosphate analog FTY720 does not improve fracture healing in mice, Journal of orthopaedic research : official publication of the Orthopaedic Research Society 31(11) (2013) 1845-50.

[22] S. Bergdolt, A. Kovtun, Y. Hagele, A. Liedert, T. Schinke, M. Amling, M. Huber-Lang, A. Ignatius, Osteoblast-specific overexpression of complement receptor C5aR1 impairs fracture healing, PLoS One 12(6) (2017) e0179512.

[23] E. Wehrle, A. Liedert, A. Heilmann, T. Wehner, R. Bindl, L. Fischer, M. Haffner-Luntzer, F. Jakob, T. Schinke, M. Amling, A. Ignatius, The impact of low-magnitude high-frequency vibration on fracture healing is profoundly influenced by the oestrogen status in mice, Dis Model Mech 8(1) (2015) 93-104.

[24] N.A. Sims, S. Dupont, A. Krust, P. Clement-Lacroix, D. Minet, M. Resche-Rigon, M. Gaillard-Kelly, R. Baron, Deletion of estrogen receptors reveals a regulatory role for estrogen receptors-beta in bone remodeling in females but not in males, Bone 30(1) (2002) 18-25.

[25] L. Claes, M. Reusch, M. Gockelmann, M. Ohnmacht, T. Wehner, M. Amling, F.T. Beil, A. Ignatius, Metaphyseal fracture healing follows similar biomechanical rules as diaphyseal healing, Journal of orthopaedic research : official publication of the Orthopaedic Research Society 29(3) (2011) 425-32.

[26] L. Claes, S. Wolf, P. Augat, [Mechanical modification of callus healing], Der Chirurg; Zeitschrift fur alle Gebiete der operativen Medizen 71(9) (2000) 989-94.

[27] L.E. Claes, C.A. Heigele, Magnitudes of local stress and strain along bony surfaces predict the course and type of fracture healing, J Biomech 32(3) (1999) 255-66.

[28] Y. Huang, X. Zhang, K. Du, F. Yang, Y. Shi, J. Huang, T. Tang, D. Chen, K. Dai, Inhibition of beta-catenin signaling in chondrocytes induces delayed fracture healing in mice, Journal of orthopaedic research : official publication of the Orthopaedic Research Society 30(2) (2012) 304-10.

[29] A.E. Borjesson, M.K. Lagerquist, S.H. Windahl, C. Ohlsson, The role of estrogen receptor alpha in the regulation of bone and growth plate cartilage, Cell Mol Life Sci 70(21) (2013) 4023-37.

[30] P. Strube, M. Mehta, A. Baerenwaldt, J. Trippens, C.J. Wilson, A. Ode, C. Perka, G.N. Duda, G. Kasper, Sex-specific compromised bone healing in female rats might be associated with a decrease in mesenchymal stem cell quantity, Bone 45(6) (2009) 1065-72.

[31] P. Dovjak, S. Dorfer, U. Foger-Samwald, S. Kudlacek, R. Marculescu, P. Pietschmann, Serum levels of sclerostin and dickkopf-1: effects of age, gender and fracture status, Gerontology 60(6) (2014) 493-501.

Figures

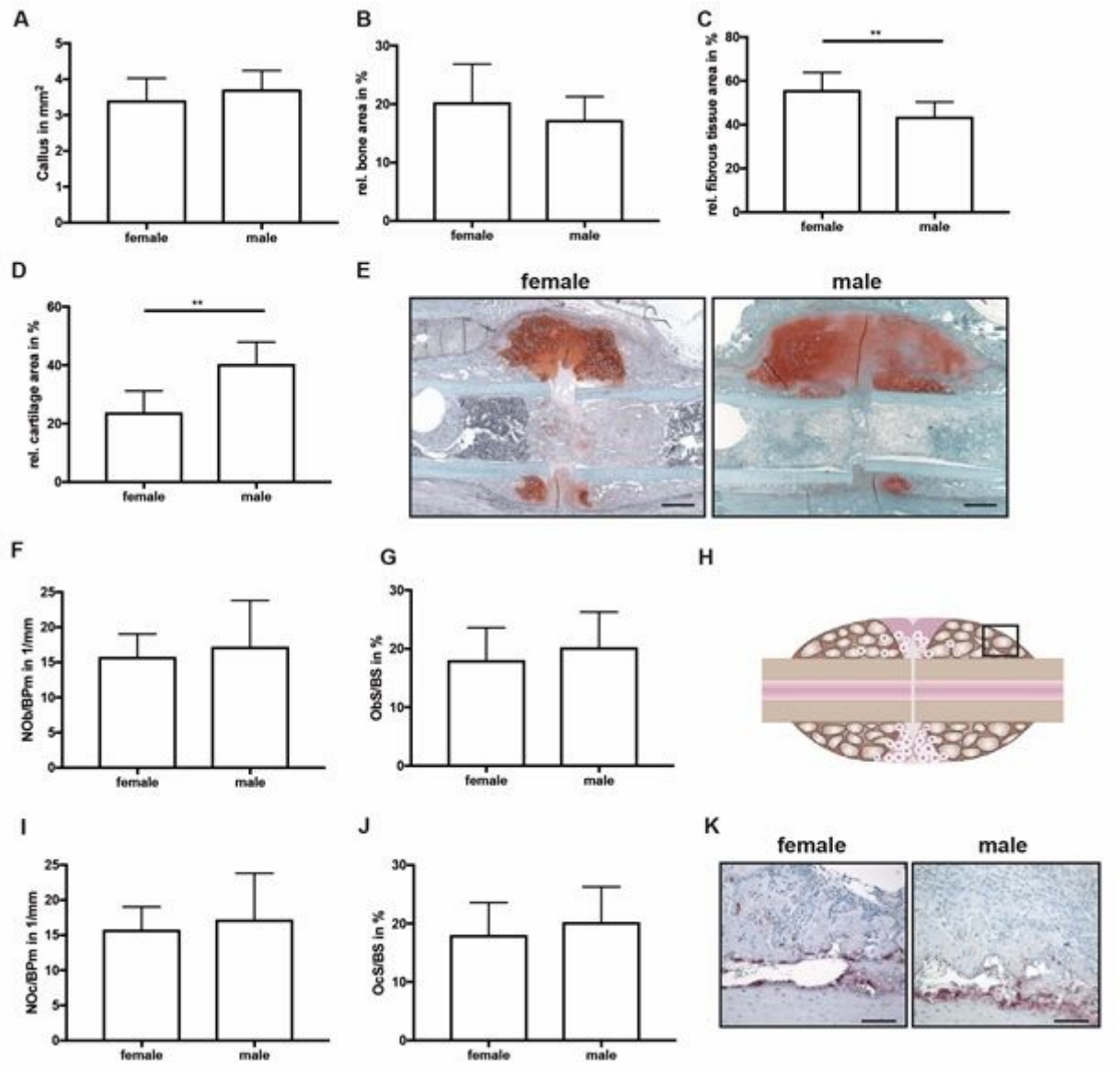

Figure 1

Histomorphometrical analysis of fractured femurs at day 10 after fracture. Analysis was performed of the entire fracture callus between the two inner pin holes. A) Whole callus tissue area, B) relative bone area, C) relative fibrous tissue area and D) relative cartilage area within the whole fracture callus at day 10 after fracture as determined by Safranin O staining. E) Representative images from Safranin O staining

of the fractured femurs. Scale bar = 500 µm. F) Number of osteoblasts per bone perimeter and G) osteoblast surface per bone surface in the bony fracture callus at day 10 after fracture as determined by Safranin O staining. H) Schematic illustration of the region of interest (black box) for osteoclast and osteoblast analysis. I) Number of osteoclasts per bone perimeter and J) osteoclast surface per bone surface in the bony fracture callus at day 10 after fracture as determined by TRAP staining. K) Representative images from TRAP staining of the bony fracture callus. Scale bar = 50 µm.

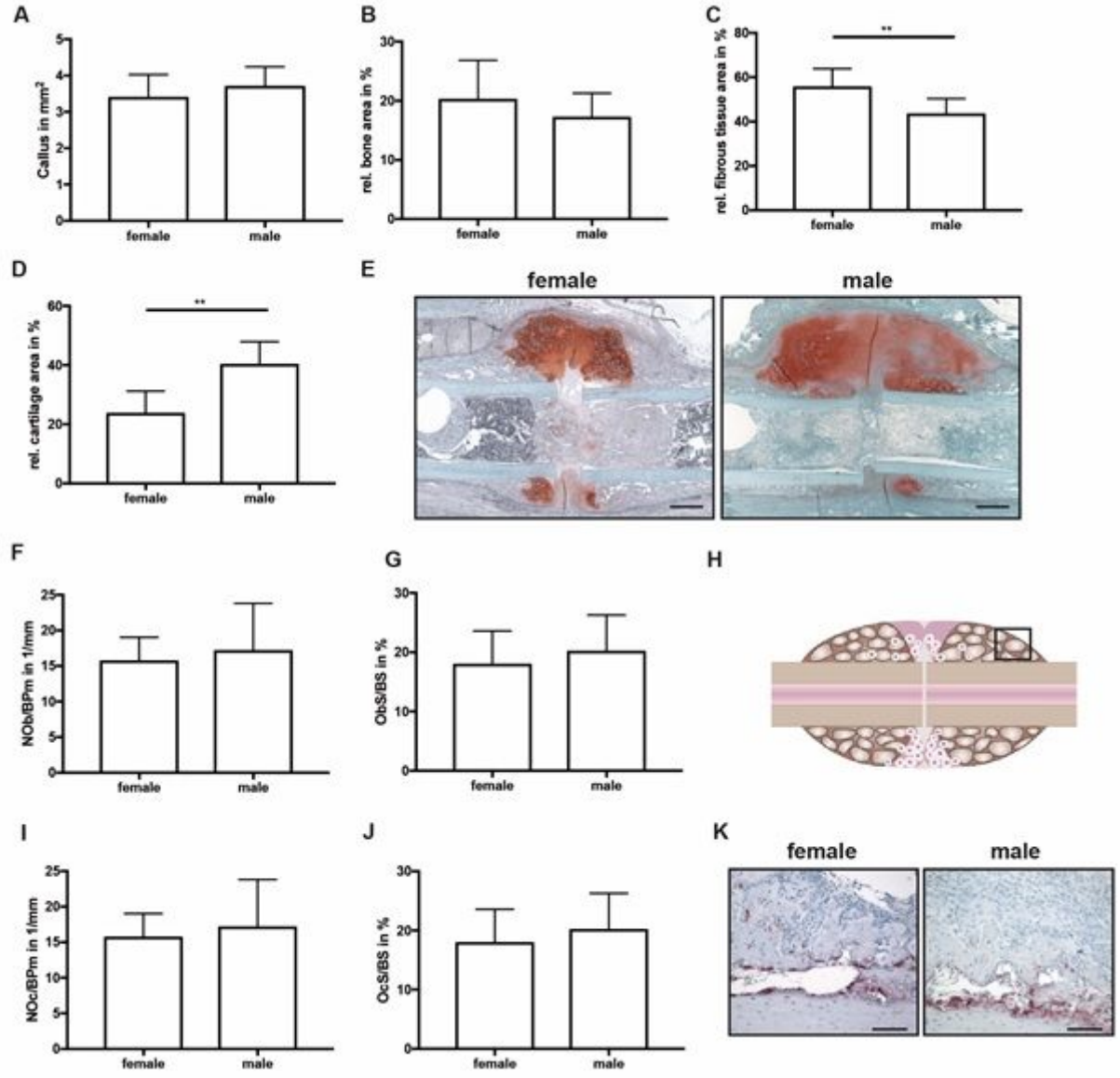

Figure 1

Histomorphometrical analysis of fractured femurs at day 10 after fracture. Analysis was performed of the entire fracture callus between the two inner pin holes. A) Whole callus tissue area, B) relative bone area, C) relative fibrous tissue area and D) relative cartilage area within the whole fracture callus at day 10 after fracture as determined by Safranin O staining. E) Representative images from Safranin O staining of the fractured femurs. Scale bar = 500 µm. F) Number of osteoblasts per bone perimeter and G) osteoblast surface per bone surface in the bony fracture callus at day 10 after fracture as determined by Safranin O staining. H) Schematic illustration of the region of interest (black box) for osteoclast and

osteoblast analysis. I) Number of osteoclasts per bone perimeter and J) osteoclast surface per bone surface in the bony fracture callus at day 10 after fracture as determined by TRAP staining. K) Representative images from TRAP staining of the bony fracture callus. Scale bar = 50 µm.

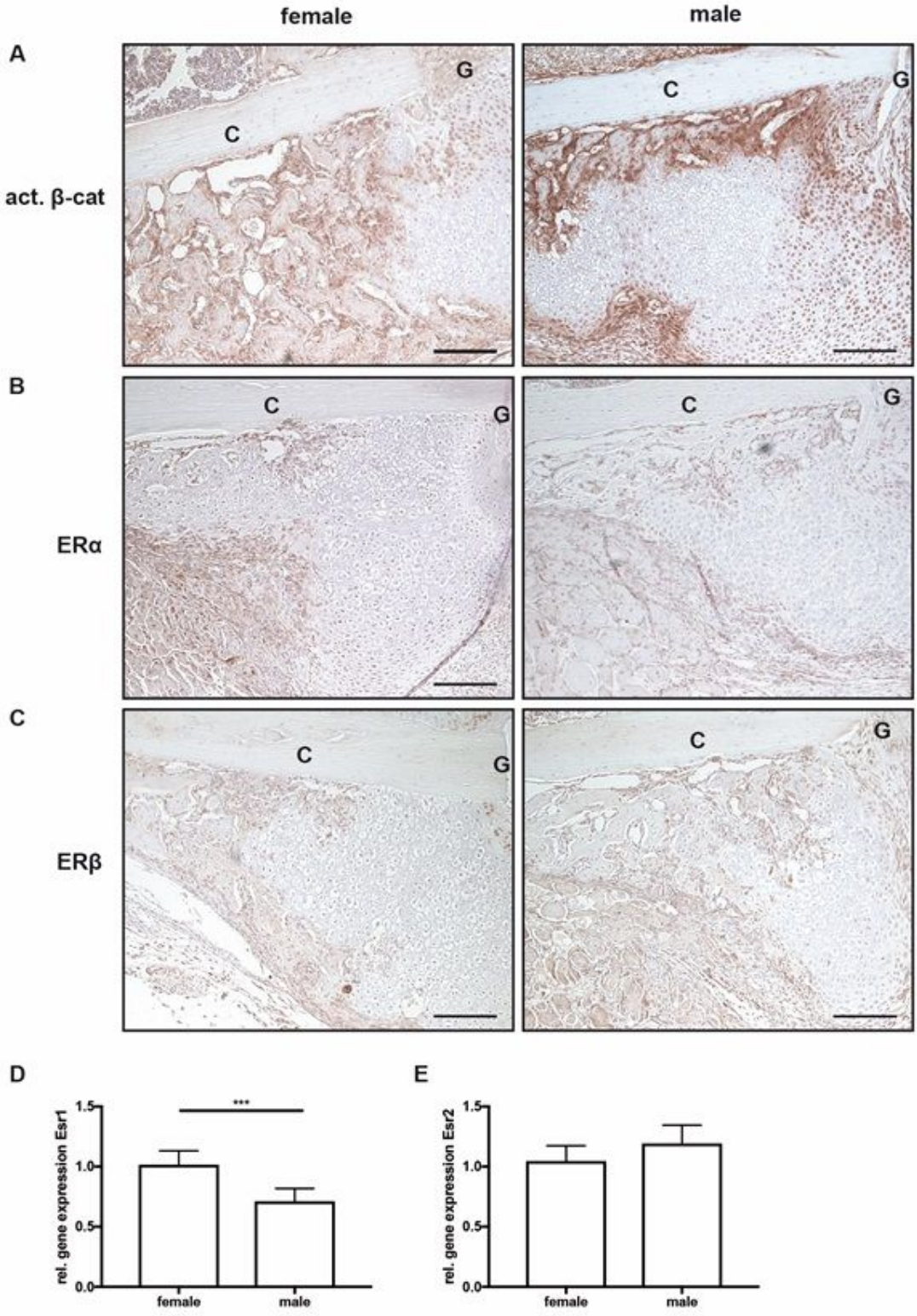

Figure 2

Immunohistochemical staining and gene expression analysis of fractured femurs at day 10 after fracture. Representative images from fractured femurs stained for A) active β-catenin, B) oestrogen receptor α

(ERα) and C) oestrogen receptor β (ERβ). Relative gene expression of D) Esr1 (ERα) and C) Esr2 (ERβ) as analysed by qPCR from whole fractured femur sections. Scale bar = 300 µm. C = cortex. G = fracture gap.

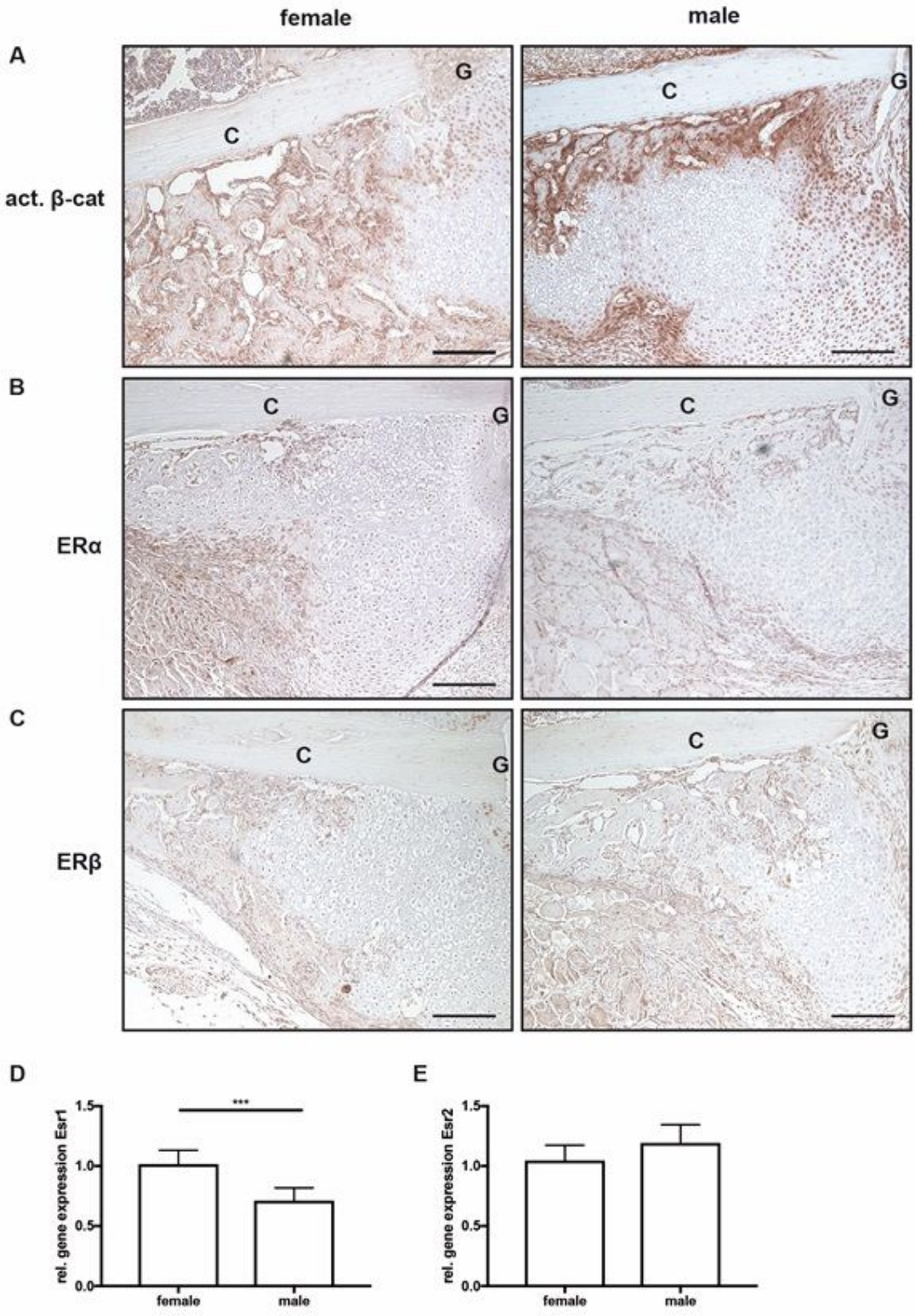

Figure 2

Immunohistochemical staining and gene expression analysis of fractured femurs at day 10 after fracture. Representative images from fractured femurs stained for A) active β-catenin, B) oestrogen receptor α

(ERα) and C) oestrogen receptor β (ERβ). Relative gene expression of D) Esr1 (ERα) and C) Esr2 (ERβ) as analysed by qPCR from whole fractured femur sections. Scale bar = 300 µm. C = cortex. G = fracture gap.

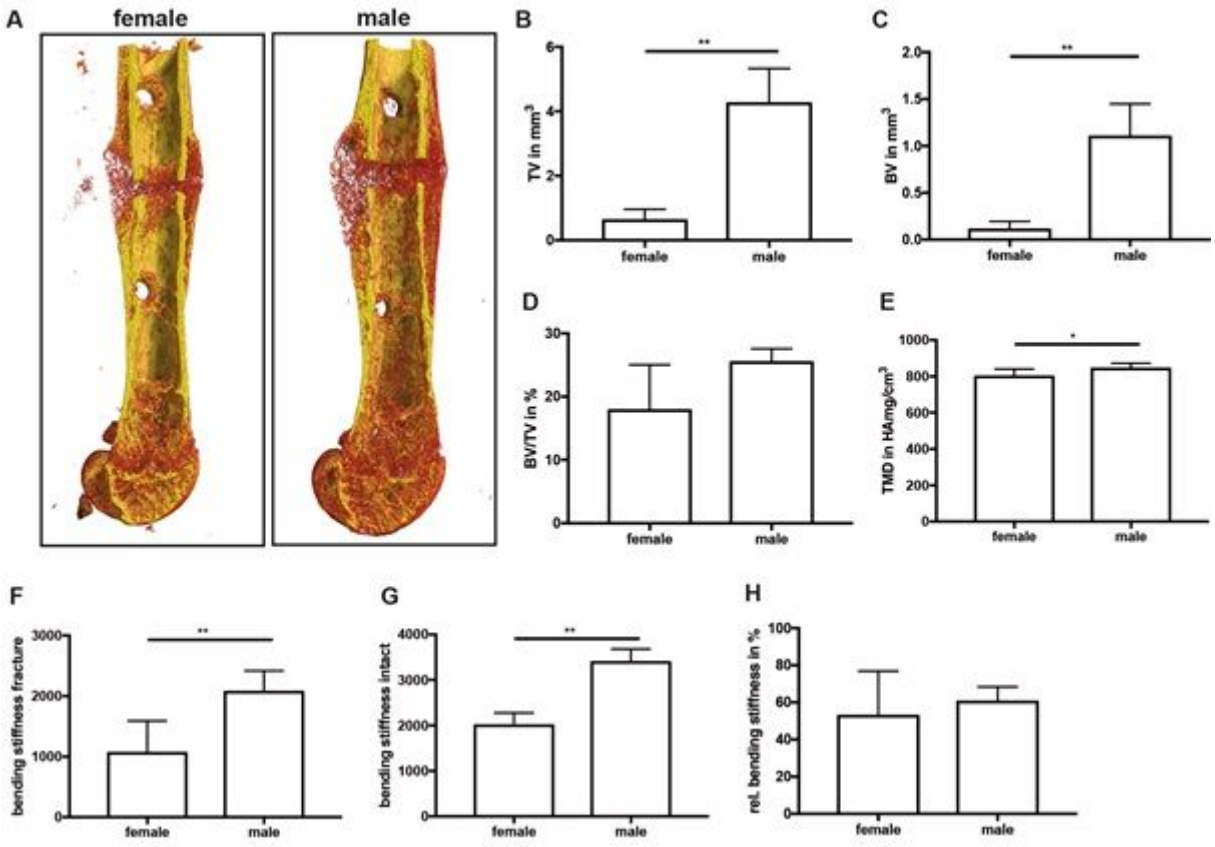

Figure 3

µCT analysis and biomechanical testing of fractured femurs at day 21 after fracture. A) Representative 3D images of fractured femurs were generated automatically by the programme CTVox and the standard transfer function for bone and metal. BMD calibration showing less mineralised areas in red, whereas highly mineralised areas are displayed in yellow. B) Callus tissue volume, C) bone tissue volume, D) bone volume ratio and E) tissue mineral density in the fracture gap at day 21 after fracture. F) Bending stiffness of fractured femurs, G) bending stiffness of intact femurs and H) relative bending stiffness of the fractured femur at day 21 after fracture.

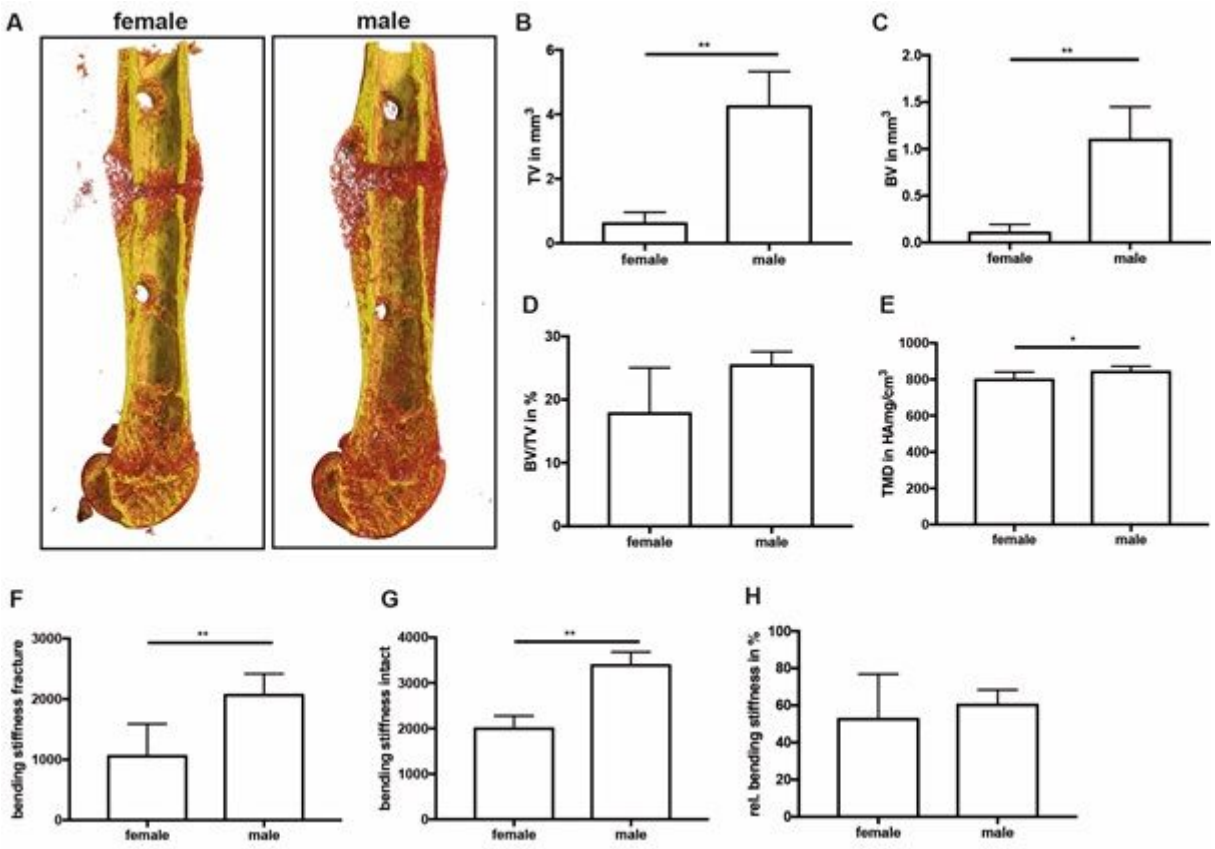

Figure 3

µCT analysis and biomechanical testing of fractured femurs at day 21 after fracture. A) Representative 3D images of fractured femurs were generated automatically by the programme CTVox and the standard transfer function for bone and metal. BMD calibration showing less mineralised areas in red, whereas highly mineralised areas are displayed in yellow. B) Callus tissue volume, C) bone tissue volume, D) bone volume ratio and E) tissue mineral density in the fracture gap at day 21 after fracture. F) Bending stiffness of fractured femurs, G) bending stiffness of intact femurs and H) relative bending stiffness of the fractured femur at day 21 after fracture.

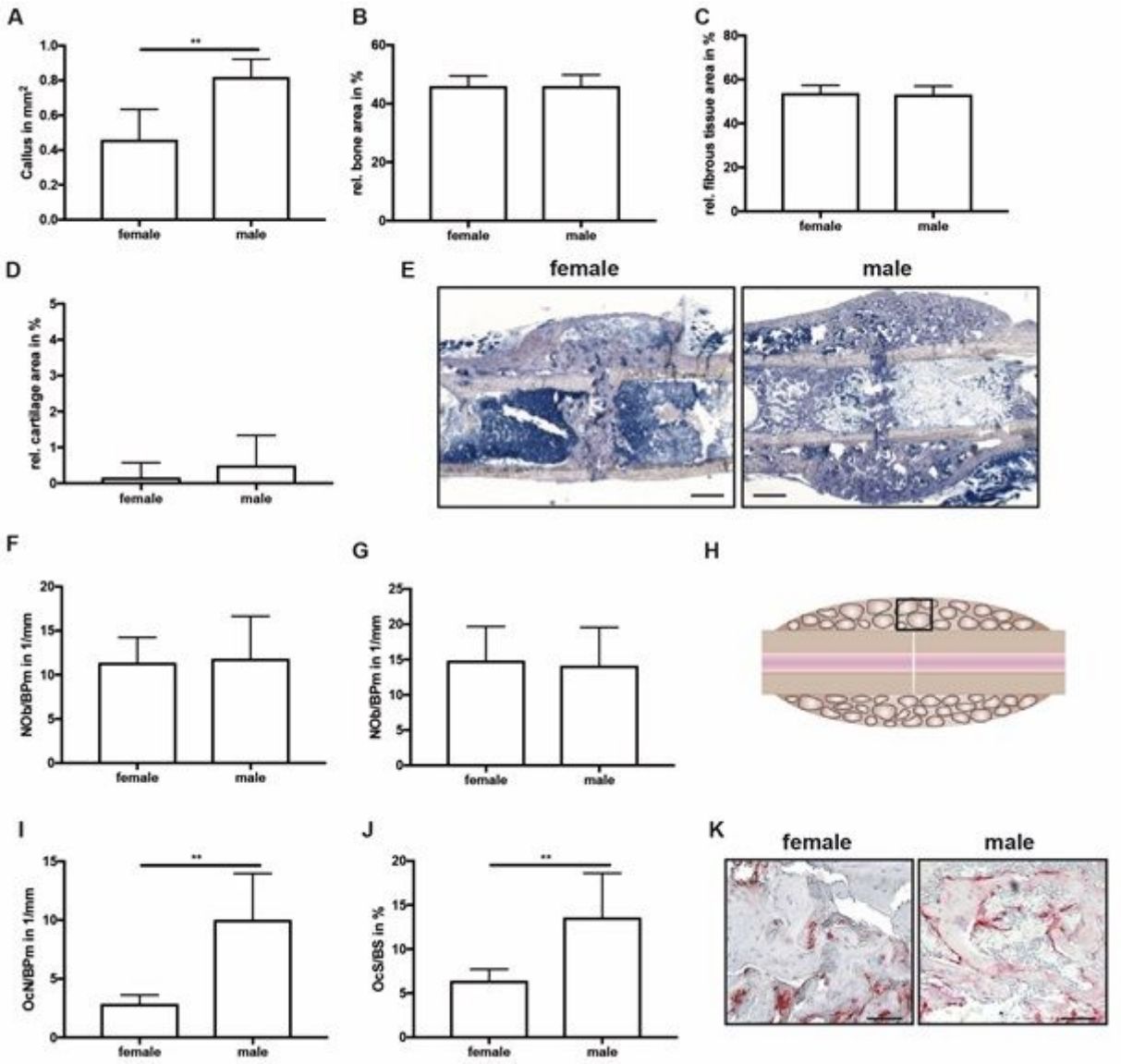

Figure 4

Histomorphometrical analysis of fractured femurs at day 21 after fracture. Analysis was performed of the entire fracture callus between the two fractured cortices (gap). A) Whole callus tissue area, B) relative bone area, C) relative fibrous tissue area and D) relative cartilage area in the whole fracture callus at day 21 after fracture as determined by Giemsa staining. E) Representative images from Giemsa staining of the fracture callus. Scale bar = 500 µm. F) Number of osteoblasts per bone perimeter and G) osteoblast surface per bone surface in the bony fracture callus at day 21 after fracture as determined by Giemsa staining. H) Schematic illustration of the region of interest (black box) for osteoclast and osteoblast analysis. I) Number of osteoclasts per bone perimeter and J) osteoclast surface per bone surface in the bony fracture callus at day 21 after fracture as determined by TRAP staining. K) Representative images from TRAP staining of the bony fracture callus. Scale bar = 50 µm.

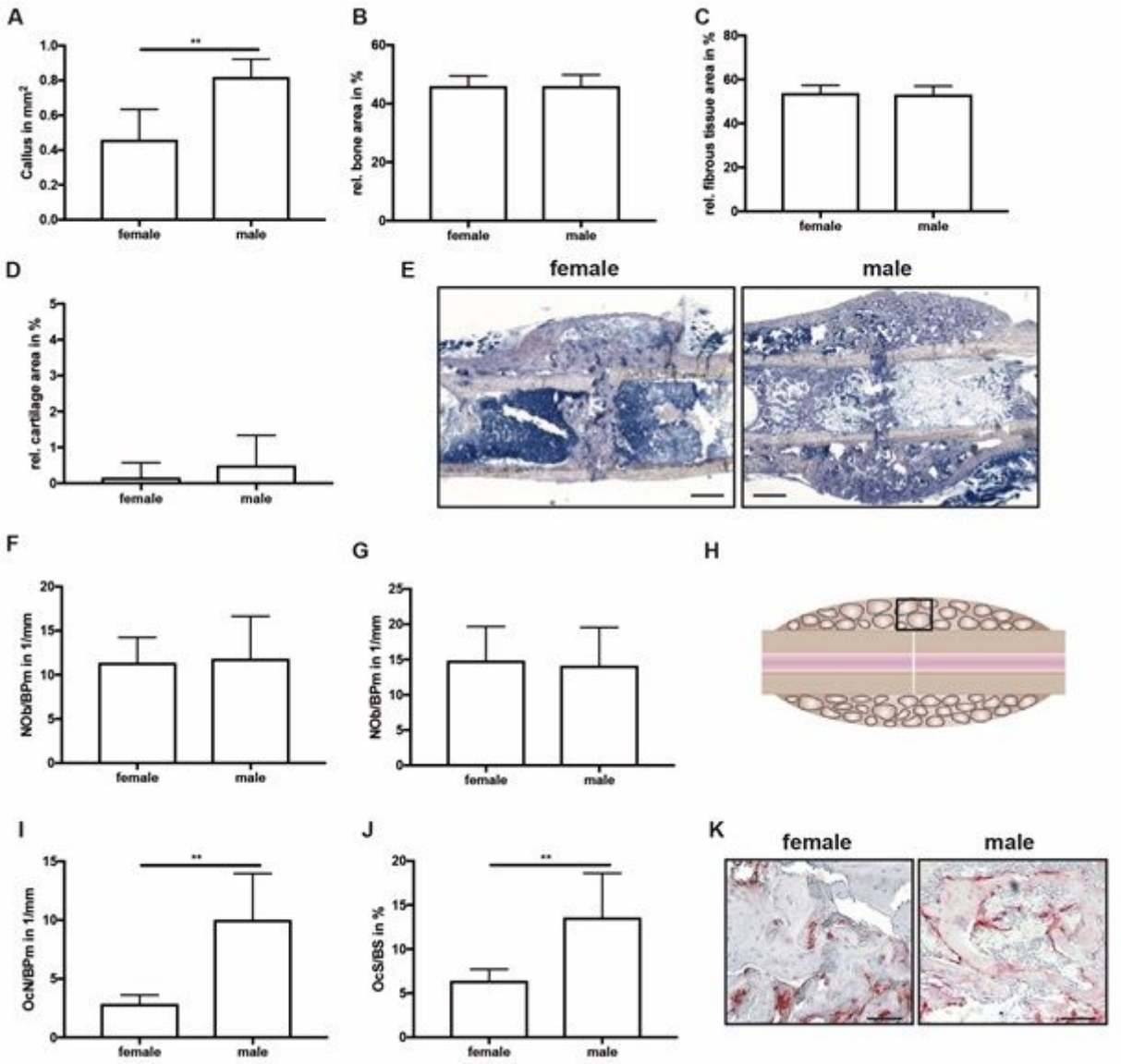

Figure 4

Histomorphometrical analysis of fractured femurs at day 21 after fracture. Analysis was performed of the entire fracture callus between the two fractured cortices (gap). A) Whole callus tissue area, B) relative bone area, C) relative fibrous tissue area and D) relative cartilage area in the whole fracture callus at day 21 after fracture as determined by Giemsa staining. E) Representative images from Giemsa staining of the fracture callus. Scale bar = 500 µm. F) Number of osteoblasts per bone perimeter and G) osteoblast surface per bone surface in the bony fracture callus at day 21 after fracture as determined by Giemsa staining. H) Schematic illustration of the region of interest (black box) for osteoclast and osteoblast analysis. I) Number of osteoclasts per bone perimeter and J) osteoclast surface per bone surface in the bony fracture callus at day 21 after fracture as determined by TRAP staining. K) Representative images from TRAP staining of the bony fracture callus. Scale bar = 50 µm.